Molecular dynamics simulations of the [2Fe-2S] cluster-binding domain of NEET proteins reveal key molecular determinants that induce their cluster transfer/release

Luca Pesce[1], Vania Calandrini[1], Henri-baptiste Marjault[2], Colin H. Lipper[3], Gulia Rossetti[1,4,5], Ron Mittler[6], Patricia A. Jennings[3], Andreas Bauer[7], Rachel Nechushtai[2*] and Paolo Carloni[1,8*]

1.Computational Biomedicine Section, Institute of Advanced Simulation (IAS-5) and Institute of Neuroscience and Medicine (INM-9), Forschungszentrum Jülich GmbH, 52425 Jülich, Germany.
2.The Alexander Silberman Life Science Institute and the Wolfson Center for Applied Structural Biology, The Hebrew University of Jerusalem, Edmond J. Safra Campus at Givat Ram, Jerusalem 91904, Israel.
3. Departments of Chemistry and Biochemistry, University of California San Diego, La Jolla, CA, 92093, United States of America.
4. Division Computational Science - Simulation Laboratory Biology, Jülich Supercomputing Centre (JSC), Forschungszentrum Jülich GmbH, 52428 Jülich, Germany.
5. Department of Oncology, Hematology and Stem Cell Transplantation, University Hospital Aachen, RWTH Aachen University, 52074 Aachen, Germany.
6. Department of Biological Sciences and BioDiscovery Institute, University of North Texas, Denton, Texas, United States of America.
7. Molecular Organisation of the Brain Molecular Neuroimaging, Institute of Neuroscience and Medicine (INM-2), Forschungszentrum Jülich GmbH, 52428 Jülich, Germany
8. JARA-HPC, 52428 Jülich, Germany

*corresponding authors rachel@mail.huji.ac.il and p.carloni@fz-juelich.de

Supporting information

S1 Model Systems

Figure S1 shows the model systems used in the parameterization of the force field of the [2Fe-2S] cluster-binding domain (see 2.1).

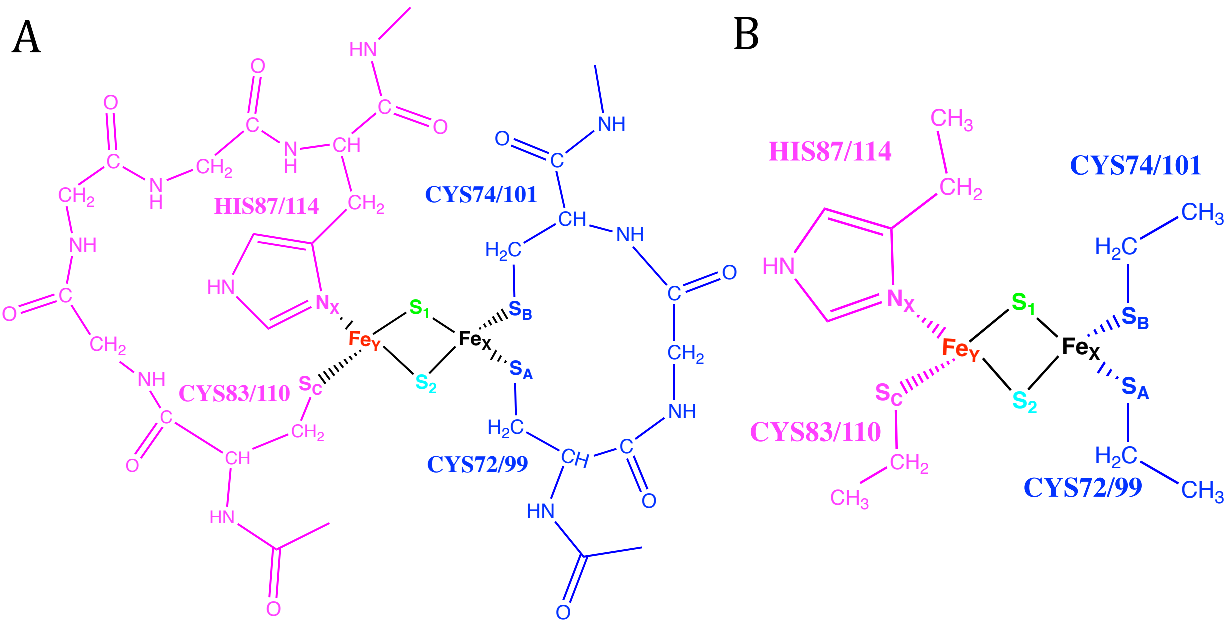

Figure S1
NEET proteins' cluster-binding domain parametrization. Models **I** (A) and **II** (B) for which QM calculations have been carried out.

S2. Results

S2.1 Parameters of the protein cluster-binding domain

Here we present the Amber-like force field parameters for the [2Fe-2S] cluster for NAF-1 and mNT, in their His:N_ε protonated state and deprotonated states (Tables S1-3).

We notice the following: (i) The bond force constant parameters are one order of magnitude smaller than those related to the covalent bonds[1a] (Tables S1-S2). This has been also seen in ref. [2]. (ii) The partial charges compare well with the partial charges estimated for the 4Cys coordination set of the [2Fe-2S] cluster-binding domain of Ferredoxin[2] (detailed in Table S3).

Table S1

Bond parameters of the His-protonated cluster. Bond stretching (A) and bending (B) parameters. S_1 and S_2 are the bridges sulfur of the iron sulfur clusters while S_A (Cys72/99:S_γ), S_B (Cys74/101:S_γ), S_C (Cys83/110:S_γ) and N_X (His87/114:N_δ) are the coordinating atoms of the protein (See Figure S1).

A

Bond	r_{min} [nm]	K_r [kJ/(mol nm^2)]	Bond	r_{min} [nm]	K_r [kJ/(mol nm^2)]
Fe_X-S_1	0.23689	20585.3	Fe_X-S_A	0.23048	33513.8
Fe_X-S_2	0.23443	22970.2	Fe_X-S_B	0.23142	33388.3
Fe_Y-S_1	0.22467	36610.0	Fe_Y-S_C	0.23341	29706.4
Fe_Y-S_2	0.22552	35982.4	Fe_Y-N_X	0.21767	16777.8

B

Angle	θ_{min} [deg]	K_θ [kJ/(mol deg^2)]	Angle	θ_{min} [deg]	K_θ [kJ/(mol deg^2)]
S_A-Fe_X-S_1	110.9	143.595	S_C-Fe_Y-S_1	116.3	240.915
S_A-Fe_X-S_2	113.9	173.259	S_C-Fe_Y-S_2	119.3	238.07
S_B-Fe_X-S_1	113.5	181.084	N_X-Fe_Y-S_1	112.4	200.665
S_B-Fe_X-S_2	113.8	195.811	N_X-Fe_Y-S_2	119.3	238.07
S_A-Fe_X-S_B	108.6	113.303	S_C-Fe_Y-N_X	100.5	124.516
S_1-Fe_X-S_2	95.8	396.811	S_1-Fe_Y-S_2	102.0	336.184
Fe_X-S_1-Fe_Y	80.9	259.157	Fe_X-S_2-Fe_Y	81.3	251.835
C_β-S_A-Fe_X	103.5	262.672	C_β-S_B-Fe_X	102.8	267.818
C_β-S_C-Fe_Y	104.8	332.084	C_γ-N_X-Fe_Y	131.9	288.863
C_ϵ-N_X-Fe_Y	120.1	296.771			

Table S2

Bond parameters of the His-deprotonated cluster. Bond stretch (A) and bending (B) parameters. Labels as in Table S1.

A

Bond	r_{min} [nm]	K_r [kJ/(mol nm^2)]	Bond	r_{min} [nm]	K_r [kJ/(mol nm^2)]
Fe_X-S_1	0.22638	34476.2	Fe_X-S_A	0.23574	27488.9
Fe_X-S_2	0.22600	34894.6	Fe_X-S_B	0.23443	29539.0
Fe_Y-S_1	0.22433	37572.3	Fe_Y-S_C	0.23560	27572.6
Fe_Y-S_2	0.22476	37656.0	Fe_Y-N_X	0.20590	30375.8

B

Angle	θ_{min} [deg]	K_θ [kJ/(mol deg^2)]	Angle	θ_{min} [deg]	K_θ [kJ/(mol deg^2)]
S_A-Fe_X-S_1	113.8	156.021	S_C-Fe_Y-S_1	109.8	201.920
S_A-Fe_X-S_2	111.7	147.779	S_C-Fe_Y-S_2	110.6	198.071
S_B-Fe_X-S_1	111.5	190.581	N_X-Fe_Y-S_1	114.9	217.568
S_B-Fe_X-S_2	113.5	190.163	N_X-Fe_Y-S_2	112.2	220.078
S_A-Fe_X-S_B	105.2	127.486	S_C-Fe_Y-N_X	106.9	136.022
S_1-Fe_X-S_2	101.4	309.700	S_1-Fe_Y-S_2	102.5	317.649
Fe_X-S_1-Fe_Y	78.0	253.216	Fe_X-S_2-Fe_Y	78.0	265.558
C_β-S_A-Fe_X	104.5	274.512	C_β-S_B-Fe_X	104.1	302.210
C_β-S_C-Fe_Y	105.6	338.737	C_ϵ-N_X-Fe_Y	123.9	245.768
C_ϵ-N_X-Fe_Y	131.2	251.835			

Table S3

Partial charges of the NEET cluster-binding domain. The partial charges for the His-protonated (columns 2-5) and His-deprotonated (columns 6-9) systems, are compared to the partial charges calculated for ferredoxin 4Cys coordination system[2]. The first two rows are related to the partial charges of the atoms within the [2Fe-2S] cluster (see Figure S1). The other rows contain the different atoms of the specified amino acids in each column.

Atom									
$S_{(1/2)}$	-0.5164	-0.5953	-0.6645			-0.7557	-0.5658		
$Fe_{(x/y)}$	0.6004	0.8618	0.7015			0.7915	0.5520		
	4Cys	Cys-72(99)	Cys-74(101)	Cys-83(110)	His-87(114)	Cys-72(99)	Cys-74(101)	Cys-83(110)	His-87(114)
S (N_δ)	-0.6100	-0.6045	-0.4662	-0.6677	-0.3252	-0.6045	-0.4662	-0.6677	-0.0832
C_β	0.2159	0.0831	0.1952	0.2160	-0.5907	0.0831	0.1952	0.2160	-0.0031
H_β	-0.0493	0.0706	0.0250	0.0318	0.1735	0.0706	0.0250	0.0318	0.0475
C_α	0.3370	-0.0692	0.0429	-0.0330	0.1204	-0.0692	0.0429	-0.0330	-0.3328
H_α	-0.0443	-0.0141	0.0766	0.0162	0.0823	-0.0141	0.0766	0.0162	0.1849
$C_{\delta 2}$					-0.0582				0.2364
$H_{\delta 2}$					0.1100				0.0618
$N_{\epsilon 2}$					-0.3374				-0.6901
$H_{\epsilon 2}$					0.3725				
$C_{\epsilon 1}$					0.0338				0.2177
$H_{\epsilon 1}$					0.1980				0.0751
C_γ					0.3151				-0.1870
C	0.5973	0.5973	0.5973	0.5973	0.5973	0.5973	0.5973	0.5973	0.5973
N	-0.4157	-0.4157	-0.4157	-0.4157	-0.4157	-0.4157	-0.4157	-0.4157	-0.4157
H	0.0443	0.2719	0.2719	0.2719	0.2719	0.2719	0.2719	0.2719	0.2719
O	-0.5679	-0.5679	-0.5679	-0.5679	-0.5679	-0.5679	-0.5679	-0.5679	-0.5679

S2.2 Molecular dynamics results of NEET proteins: Additional details

RMSD of mNT and NAF-1 C_α's in their His protonated and deprotonated states. We removed the last three residues at the C-terminal of each monomer to avoid the contribution of large fluctuations due to these highly mobile domains. Figure S2 shows the results obtained for NAF-1 protonated (red colored), NAF-1 deprotonated (green colored), mNT protonated (blue colored) and mNT deprotonated (magenta colored). Figure S2.A shows the time evolution of the RMSD (running average) relative to the crystal structures[3]. Figure S2.B shows the distributions of the RMSD relative to the crystal structure. Figure S2.C shows the distributions of the RMSD relative to the most representative structure of each simulated system. In all cases the deviations from the crystal structures are below 1Å RMSD. Therefore, the systems appear to fluctuate around a structure which is not too dissimilar from the X-ray structure[3].

Other properties of mNT and NAF-1. The secondary structures (Figure S3) of NAF-1 (A His-protonated, B His-deprotonated) and of mNT (C His-protonated, D His-deprotonated) are preserved during the molecular dynamics (preserved secondary structure over the 80%). Table S4 shows the structural parameters obtained in the simulation for the two proteins and their comparison to the measured values of the crystallography solved corresponding structures[3]. Figure S4 compares the calculated ^{15}N (Figure S4.A), ^{1}H (Figure S4.B) chemical shifts (CS) of mNT in its protonated state with the experimental values[25]. Our data are in agreement with experiment: indeed the standard deviation of the difference between experiment and simulations are below the limits of the method for each chemical species[19].

Figure S5 shows the local flexibility of the two proteins in the two protomeric states. We used the so-called protein angular dispersion value (PAD)[26]. The values for the four systems are similar except for the N and C terminals and L2-domain, which are much larger than the others.

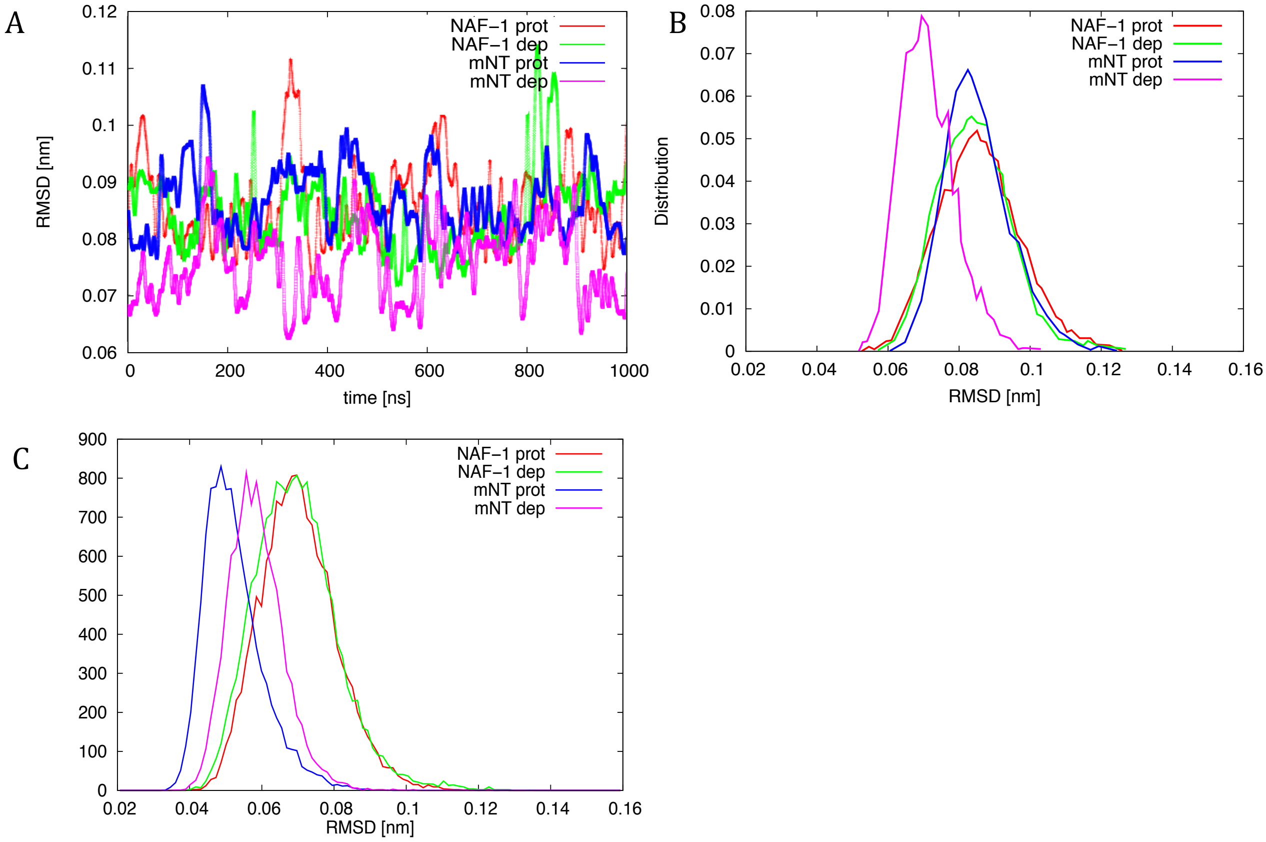

Figure S2

RMSD of the simulated proteins on 1μs of MD. (A), (B) RMSD relative to the X-ray structures[3] of the Cα of the core domain of the proteins (aa 69-132 in NAF-1, aa 43-105 in mNT). (B) Distributions of the RMSD values. (C) Distributions of the RMSD values relative to the main representative structures of the simulations. "dep" and "prot" in the legend's labels refer to the deprotonated and protonated states of the histidine coordinating to the [2Fe-2S] cluster respectively. The NAF-1 protonated is red colored, NAF-1 deprotonated is green colored, mNT protonated is blue colored and mNT deprotonated is magenta colored.

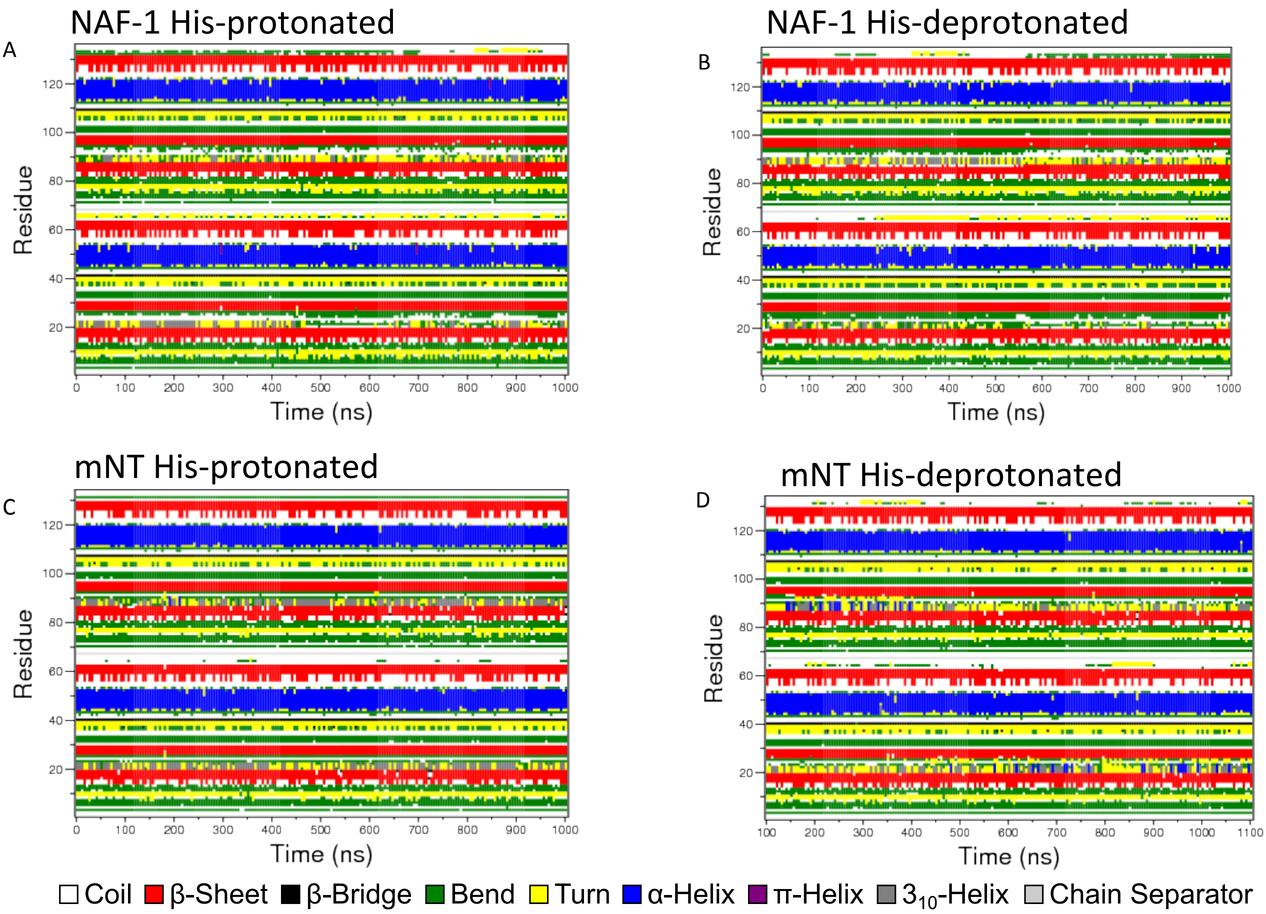

Figure S3

Secondary structures of the simulated systems. Secondary structure content (calculated as in ref.[27]) of (A) His-protonated NAF-1, (B) His-deprotonated NAF-1, (C) His-protonated mNT and (D) His-deprotonated mNT, plotted as a function of simulated time. The average contents are reported in Table S5.

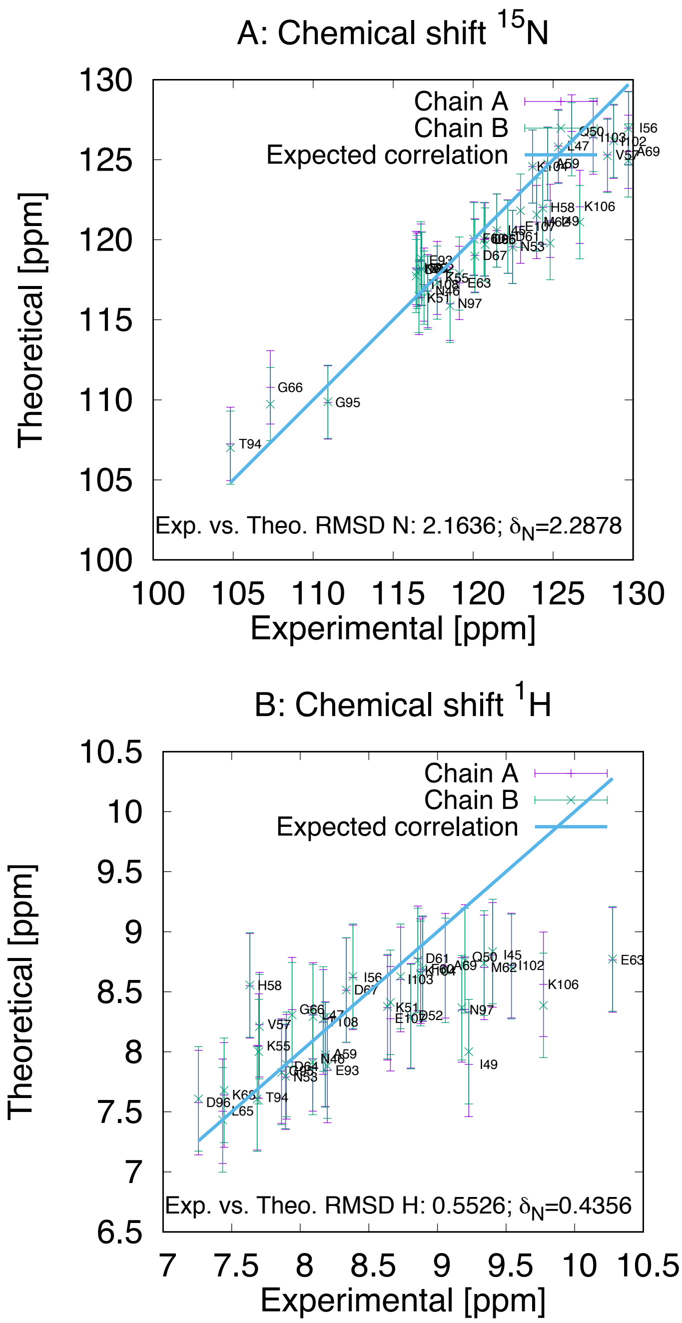

Figure S4

Comparison between experimental[25] and calculated ^{15}N (A), ^{1}H (B) NMR chemical shifts of mNT. Error bars are assigned accordingly to SHIFTX2 RMSE[19]. The experimental value is compared with the estimation for monomer A (violet) and monomer B (green).

Table S4

Structural parameters within the cluster binding domain. Comparison between the MD-averaged distances of mNT and NAF-1 proteins in both their protonation states and the values measured in the X-ray structures [3].

D[Å]	mNT dep	mNT prot	NAF-1 dep	NAF-1 prot	mNT Xray	NAF-1 Xray
S_1-Fe_1	2.19±0.08	2.21±0.09	2.19±0.08	2.19±0.10	2.14	2.22
S_2-Fe_1	2.19±0.07	2.24±0.09	2.19±0.08	2.23±0.10	2.19	2.27
S_1-Fe_2	2.19±0.07	2.11±0.07	2.17±0.07	2.11±0.07	2.19	2.24
S_2-Fe_2	2.22±0.07	2.21±0.07	2.23±0.07	2.20±0.08	2.18	2.23
Fe_1-C_1:S	2.30±0.09	2.23±0.08	2.29±0.09	2.23±0.08	2.32	2.33
Fe_1-C_2:S	2.26±0.09	2.20±0.08	2.25±0.09	2.20±0.08	2.19	2.29
Fe_2-C_3:S	2.29±0.09	2.22±0.09	2.27±0.09	2.22±0.09	2.31	2.32
Fe_2-H:N	2.01±0.09	2.03±0.1	1 2.00±0.08	2.02±0.10	2.16	2.18

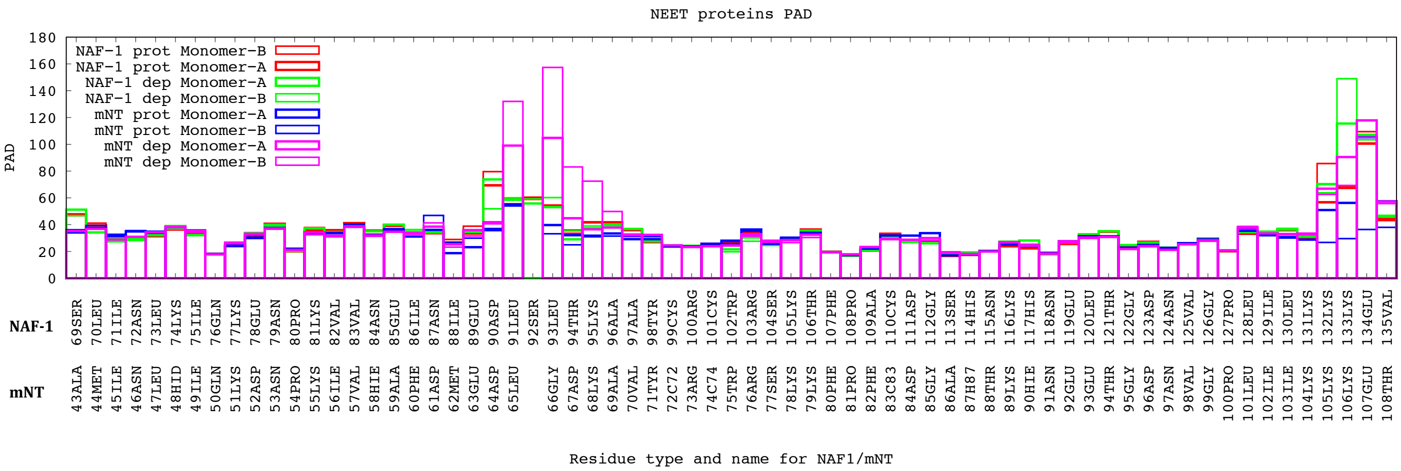

Figure S5

Flexibility of mNT and NAF-1 proteins. PAD values [17] for NAF-1(69:135) and mNT(43:108) in both protonation states. The residues are aligned accordingly to their structural overlap.

Table S5

Secondary structure content[27]**.** (A) Values for each monomer of NAF-1 without one [2Fe-2S] cluster in monomer B, apo-NAF-1, mNT without one [2Fe-2S] cluster in monomer A and apo-mNT. In the third column "X" remarks in which monomer the [2Fe-2S] cluster is contained. (B) Values for NAF-1 and mNT in their His-Protonated (His-prot) and His-Deprotonated (His-dep) states and their structures without one (-[2Fe-2S]) and two [2Fe-2S] (-2*[2Fe-2S]) clusters.

A

Protein	**Monomer**	**Cluster**	**Structure**	**Coil**	**β-Sheet**	**Turn**	**α-Helix**
NAF-1	A	X	0.33	0.42	0.11	0.15	0.06
	B		0.26	0.44	0.13	0.11	0.01
NAF-1	A		0.27	0.44	0.10	0.12	0.04
	B		0.26	0.41	0.12	0.11	0.02
mNT	A		0.32	0.42	0.12	0.14	0.05
	B	X	0.39	0.40	0.12	0.13	0.13
mNT	A		0.33	0.41	0.12	0.14	0.05
	B		0.35	0.43	0.12	0.14	0.07

B

Protein	**State**	**Structure**	**Coil**	**β-Sheet**	**Turn**	**α-Helix**
NAF-1	His-prot	0.48	0.28	0.21	0.13	0.12
	His-dep	0.46	0.29	0.21	0.12	0.12
	-[2Fe-2S]	0.36	0.37	0.18	0.13	0.03
	-2*[2Fe-2S]	0.33	0.37	0.17	0.12	0.02
mNT	His-prot	0.46	0.28	0.21	0.11	0.13
	His-dep	0.49	0.29	0.21	0.13	0.13
	-[2Fe-2S]	0.45	0.31	0.21	0.13	0.09
	-2*[2Fe-2S]	0.43	0.32	0.21	0.14	0.06

S2.3 REST2 calculations

In the REST2 simulation of the mNT-holo protein (Figure S6), the RMSD relative to the X-ray structure[3a] fluctuates below 0.2nm, similarly to what found in our plain MD simulations. RMSD and secondary structure analyses of REST2 simulations on NAF-1 with one [2Fe-2S] cluster in monomer A and apo-NAF-1 are reported in Figure S7 and S8 respectively. The same analyses for mNT with one [2Fe-2S] cluster on monomer B and apo-mNT are shown in Figure S9 and S10 respectively. Table S5 showed the secondary structure content of these systems estimated on the second half of each trajectory. The data were reported for each monomer (Table S5.A) and the entire protein, and then compared with the results obtained on the holo-states (Table S5.B). Figure S7-S10 show for each system the time evolution of the RMSD with respect to the corresponding crystal structure (panel A); the distribution of the RMSD estimated on the second half of each trajectory (panel B); the time evolution of the secondary structure (panel C); the three main representative structures of each trajectory are superimposed on the crystal structure, transparent color in (panel D). The RMSD distribution of mNT with one [2Fe-2S] cluster on monomer B (Figure S9.B) showed smaller fluctuations from its crystal structure with respect NAF-1 with one [2Fe-2S] cluster on monomer A (Figure S7.B). The reduced deviation with respect to the holo-state of mNT was also observed from the secondary structure assignment (Figure S9.C). Indeed, while there is a residual content of the α-helix on monomer A, the α-helix of monomer B is well preserved. The other secondary structure contents were more preserved with respect the holo-state (crystal structure) (see Table S5). Apo-mNT (Figure S10) showed structures that were closer by mean of RMSD (Figure S10A,B) and secondary structure (Figure S10.C and Table S5) to its folded crystal structure than Apo-NAF-1 to its crystal structure. The simulations here shown were not fully converged due to the presence of large disordered domains. Nevertheless we observed that in both proteins without one cluster the folding β-cap is highly preserved. The remarkable difference in the secondary structure content of the two proteins in their apo-states (table S5), clearly shows that mNT folding is more stable than NAF-1.

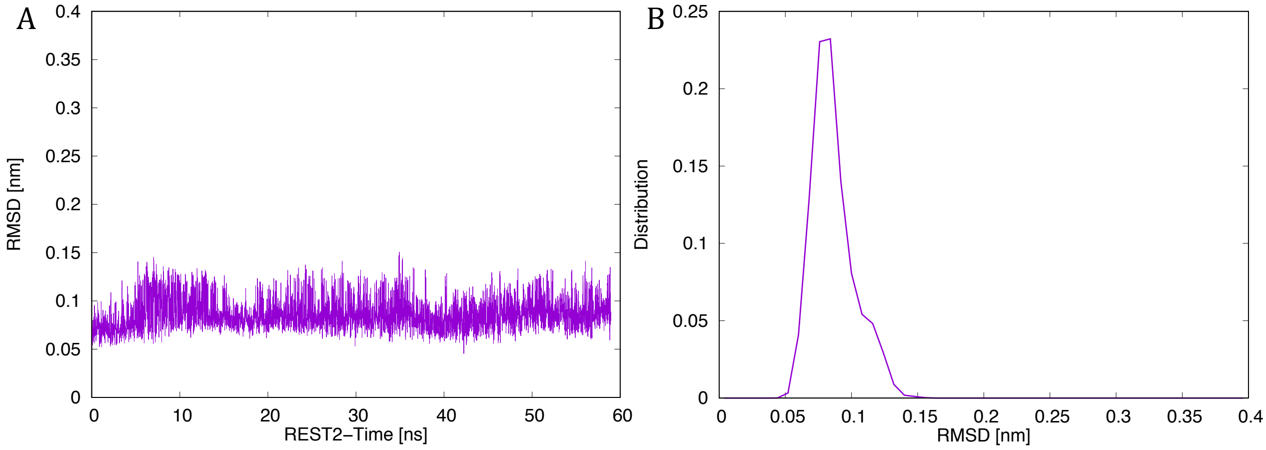

Figure S6

Test of REST2 simulation protocol on holo-mNT. (A) RMSD of Cα's of the mNT (residues 43-105), relatively to the X-ray structure[3a], plotted as a function of simulated time. (B) Distribution of the RMSD shown in (A).

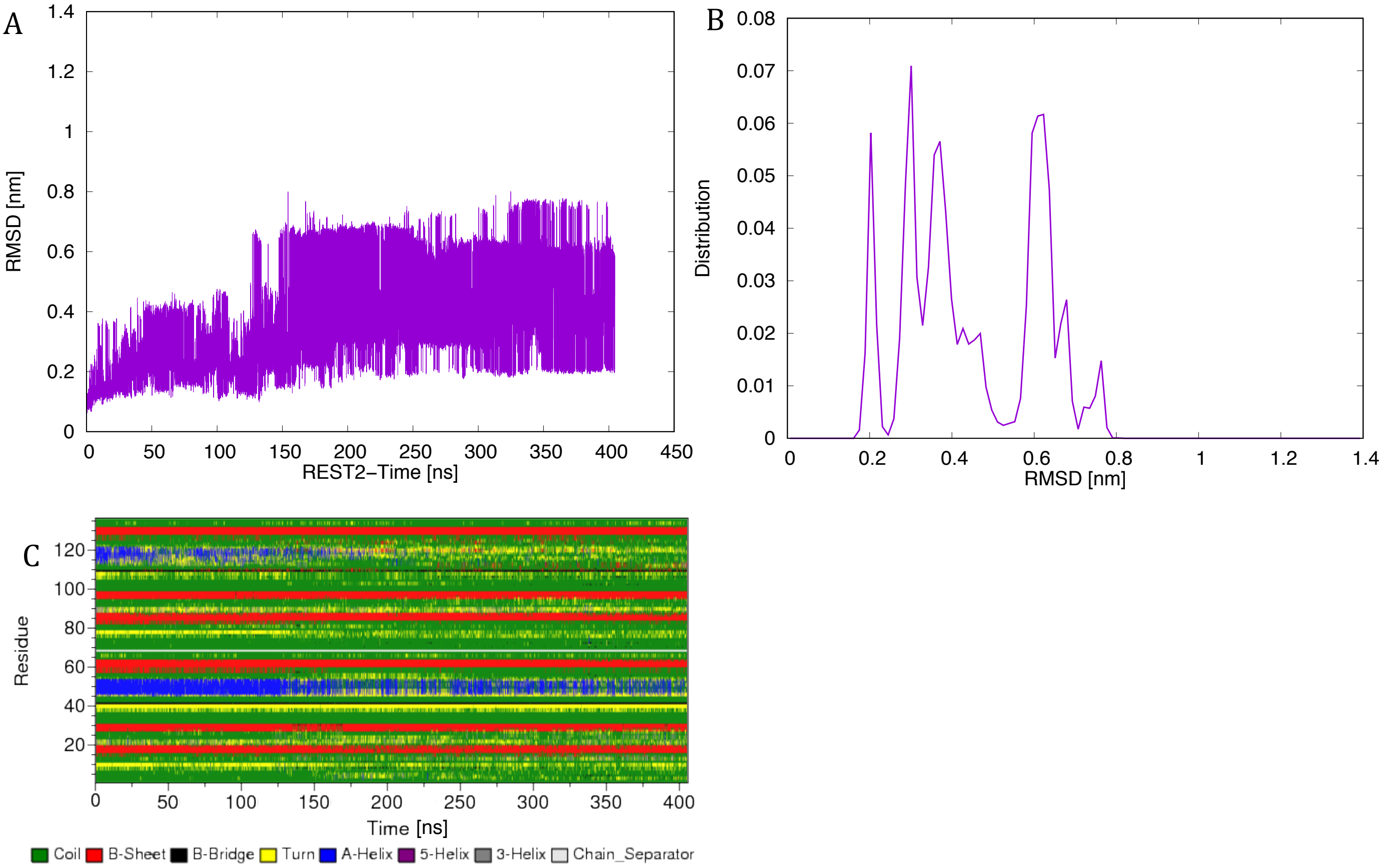

Figure S7

NAF-1 with [2Fe-2S] cluster on monomer A. (A) RMSD relative to the X-ray structure (PDB code 4OO7)[3b] of the Cα's in the core domain (residues 69-132), plotted as a function of simulated time during our MD simulation. (B) Distribution of the RMSD in the final part of the REST simulation. (C) Time evolution of the secondary structure[27]. Here, the secondary structure assignment of "Bend" secondary structures[27] has been considered together with "Coil".

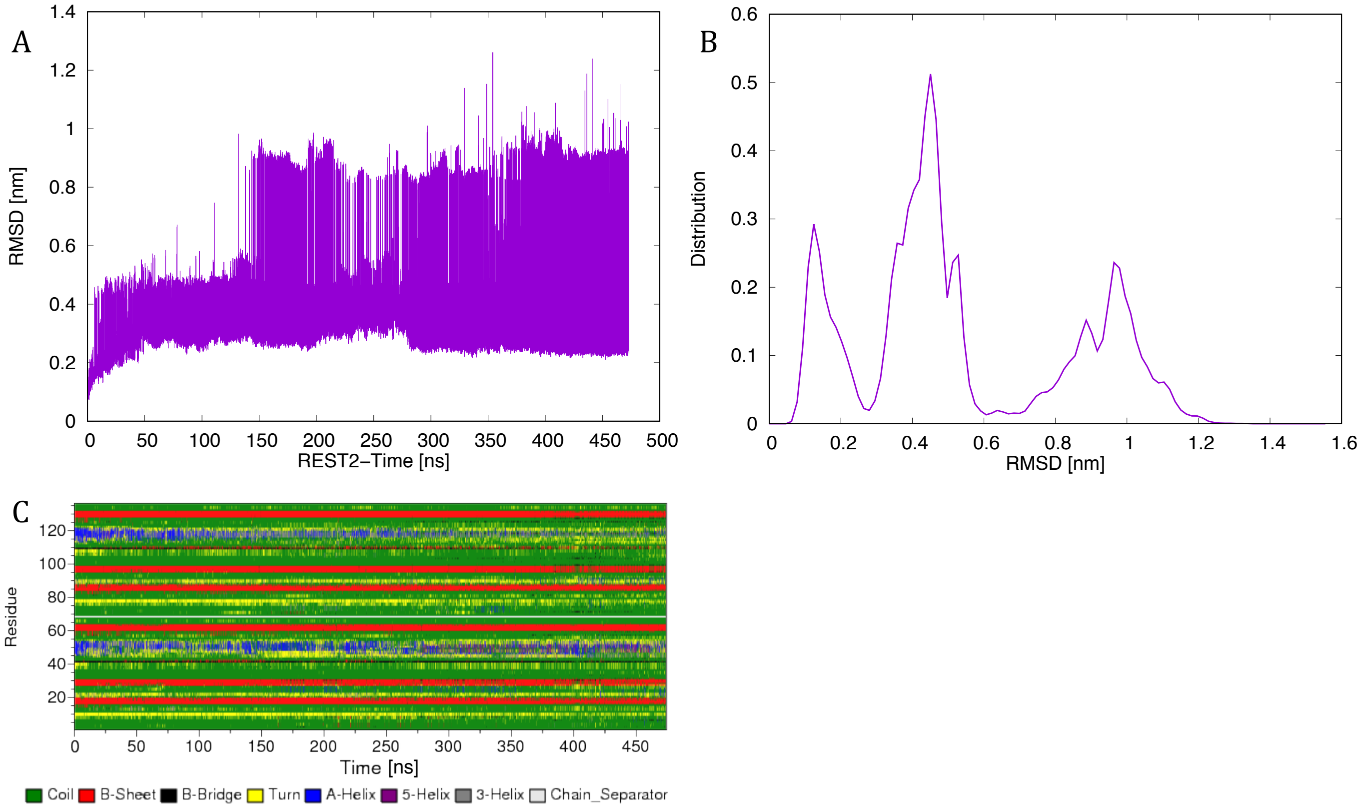

Figure S8

NAF-1 without [2Fe-2S] clusters. The descriptions of (A), (B) and (C) are analogous to Figure S7 for this studied case.

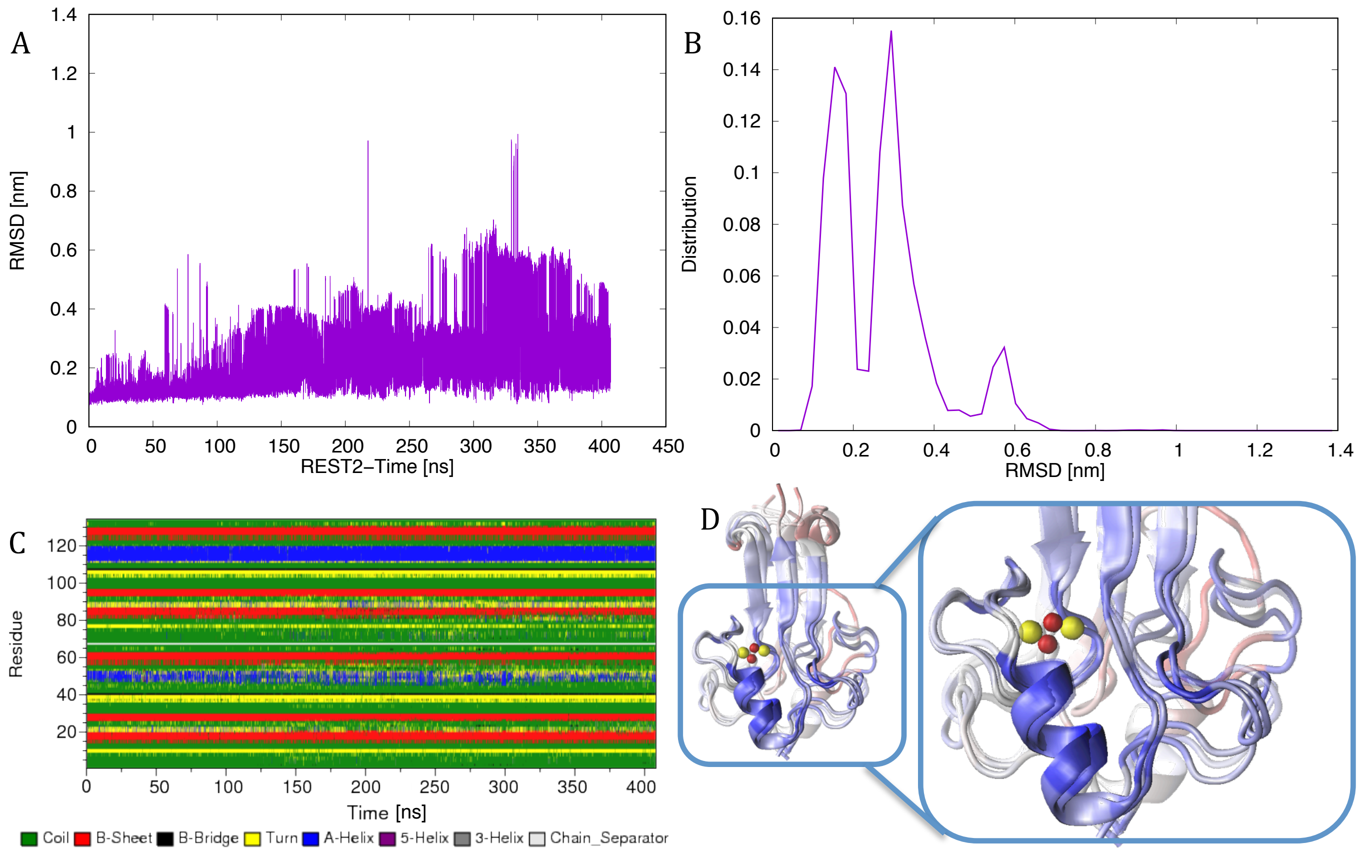

Figure S9

mNT with [2Fe-2S] cluster on monomer B. The plot reported in (A,B,D) were based only on the core domain (residues 43-105). For the description of (A), (B) and (C) see Figure S7. In this case the reference X-ray structure (PDB code 2QH7) is in ref.[3a]. (D) Superposition of the main representatives of the REST2 simulation with the corresponding X-ray structures. The color code, assigned based on the PAD analysis[17], ranges from blue (for the more rigid residues) to red (for the more flexible one).

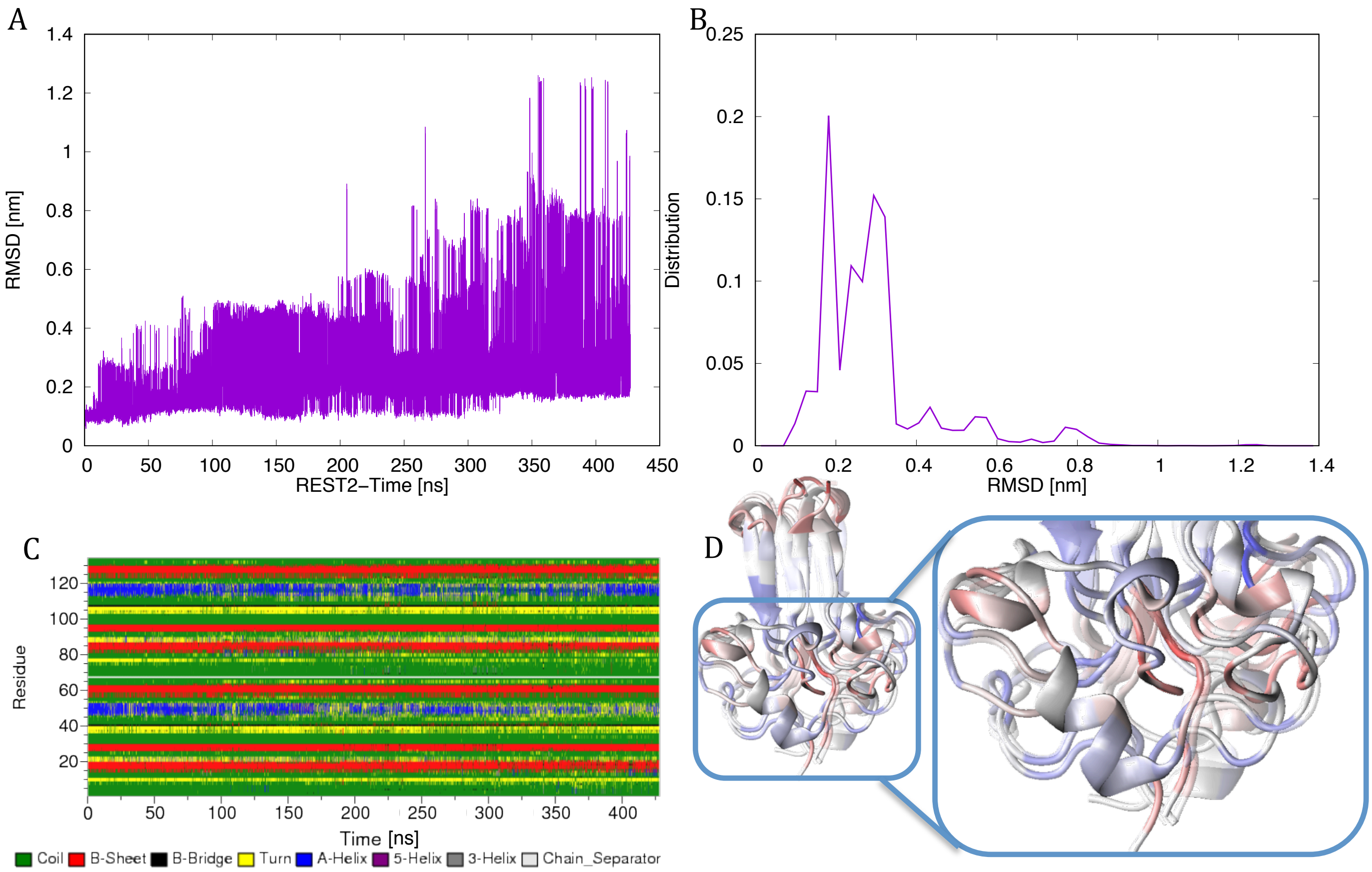

Figure S10

mNT without [2Fe-2S] clusters. The descriptions of (A), (B), (C) and (D) are analogous to Figure 9 for this studied case.

S2.5 Additional details on the cluster in NAF-1 and mNT in His-protonated/deprotonated states

Structural features. The bridging sulfur atoms (S_1, S_2) are not solvent exposed: A calculation of the radial distribution function of these atoms with the solvent shows that the shortest sulfur-water oxygen distance is 6.0Å (Fig. 12). Instead, the bridging atoms S_1 interacts with Arg73:H and Cys74:H in mNT, Arg100:H and Cys101:H in NAF-1. S_2 interacts with Asp84:H, Gly85:H, Ala87:H and His87:H in mNT, and Asp111:H, Gly112:H, Ser113:H and His114:H in NAF-1 independently on the His-protonation state. Regarding to the coordinating to the cluster, Cys83(110):S_γ formed a H-bond with water (Figure S11.B reported as cumulative distribution of the bond distance); His87(114):N_ε formed H-bond with one water oxygen in the protonated state (Figure S11.A reported as cumulative distribution of the bond distance), while in the deprotonated state it could form H-bond either with water or with the nearby Lys55(81):N_ζ (see Figure S11.A). In particular the occurrence of H-bond formation with the nearby Lys is different for the two proteins (Figure S11.C).

Electronic structure. The NBO analysis performed on NAF-1 (Table S6) and mNT (Table S7) provided similar results. In particular, in both cases the major effect on the polarization of the Fe-N bond is due to the protonation state of the coordinating HIS:N_ε.

Next, we investigated the influence of interacting groups and of the electric field on the polarity of the N_δ-Fe bond calculated using the Boys orbitals centroids (BOCs) (Table 1). The presence of the positively charged Lys in the deprotonated form makes the polarity of the bond not too dissimilar from that in the protonated form. Instead, the bond is less polar when the water molecule H-bonds to the histidine in the deprotonated form. However, this is a rather rare event, as most of the time the cluster histidine H-bond to the lysine (Figure S11.C). A significant decrease in bond-polarity upon His deprotonation however re-emerges if one includes the electrostatic field of protein and that solvent (Figure 3.D) In fact, the difference between the distances of the BOC form His114:N_δ in the His-deprotonated and His-protonated states without considering the external electric field was 0.019 and 0.026Å, for the α and β spins respectively, while following the addition of the electrostatic filed, the values were 0.041 and 0.032Å for the α and β spins respectively. In these conditions, the polarization of the His-deprotonated state does not vary depending the H-bonding partner (0.542±0.017Å for His114:N_ε-Lys:N_ζ H-bond, 0.543±0.014Å for His114:N_ε-Wat:O H-bond). In conclusion, the protonation state of the His:N_ε is the key factor that affects the bond polarization.

Table S8 reports the results obtained using the BOCs analysis on mNT. The results are similar to those obtained for NAF-1 (table D in Figure 3). Therefore, in this Section we do not add any further details to this analysis.

In absence of the protein electrostatic field, the bond order and the polarization of the N_δ-Fe bond, as emerging from the NBO analysis, are similar for the two systems (see Table S9). The addition of the protein electrostatic field (Tables S6 for NAF-1, S7 for mNT) causes a decrease in polarity (along with an increase of bond order) of the N_δ-Fe bond.

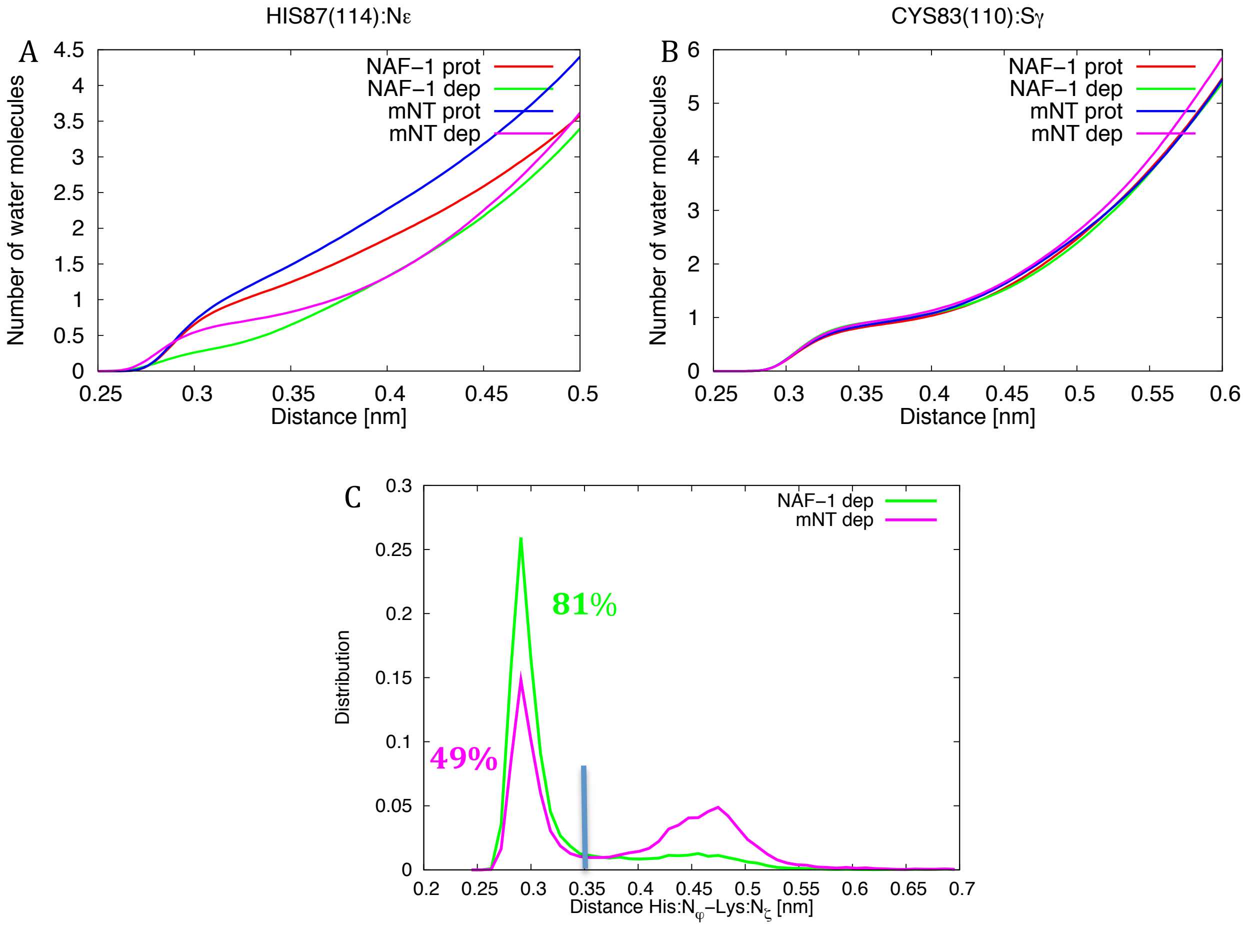

Figure S11

Hydration of the [2Fe-2S] cluster. His:N_ε-H_2O:O distance cumulative distribution function (A). Cys:C_γ-H_2O:O distance cumulative distribution function (B). Distribution of the distances between of NAF-1 His114:N_ε and the Lys81:N_ζ (green), and between mNT His87:N_ε and Lys55:N_ζ (magenta) (C). Hence, an H-bond between water and Cys110(83):S_γ in NAF-1 (mNT) is present in the systems simulated here. However, this does not affect the electronic properties calculated here (Table 3.D and S8). The two proteins here considered are in their His- N_ε deprotonated states.

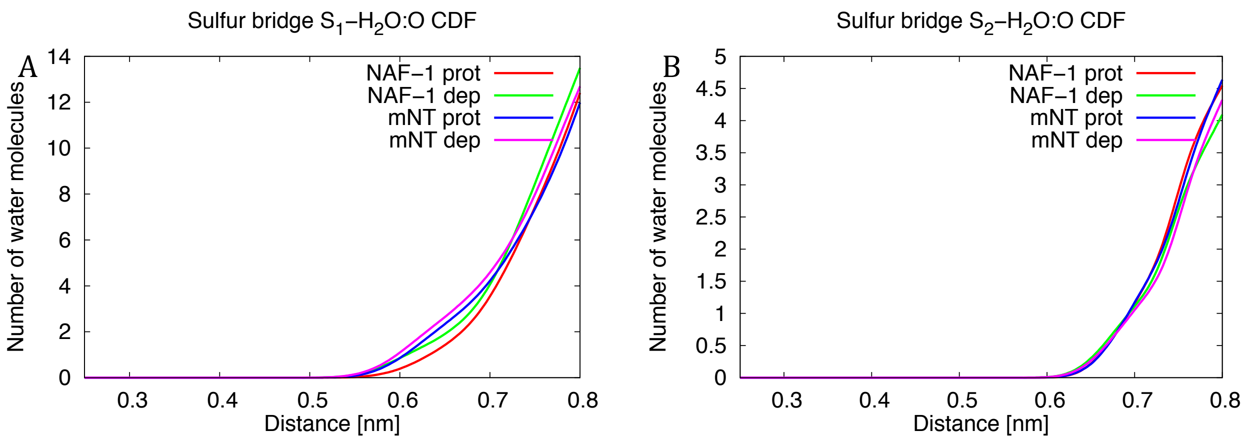

Figure S12

Hydration of the sulphur atoms of the [2Fe-2S] cluster. The number of the water molecules as function of the distance is here reported for S_1 (A) and S_2 (B) of the [2Fe-2S] cluster.

Table S6

[2Fe-2S] cluster-binding domain bond properties upon HIS:Nε protonation in the NAF-1 protein. NBO analysis[22] performed on the cluster-binding domain of NAF-1 (see methods) for the His-protonated (A) and His-deprotonated (B) states. Each row is related to a specific bond orbital estimated by the method. The first two columns are related to the protein and cofactor atoms involved in the specific bond. The third column is the spin and bond orbital order of the row. The fourth column is mean values and standard deviations of the polarization (by the mean of NBO theory) of the specific molecular orbital, and the fifth column is the occurrence ratio (see main text).

	Protein	**Cofactor**	**Spin-BO**	**Δ**	**Occurrence**
A	Protonated state				
	C_{99} S_γ	Fe_1	α_1	87.28 ± 1.12	0.99
			β_1	75.54 ± 2.24	1
			β_2	88.94 ± 1.60	0.94
	C_{101} S_γ	Fe_1	α_1	87.1 ± 1.20	0.986
			β_1	75.50 ± 1.48	1
			β_2	88.44 ± 1.92	0.97
	C_{110} S_γ	Fe_2	α_1	75.36 ± 1.57	1
			β_1	86.29 ± 0.76	1
			α_2	89.60 ± 1.94	0.93
	H_{114} N_δ	Fe_2	α_1	87.24 ± 1.16	0.98
B	Derotonated state				
	C_{99} S_γ	Fe_1	α_1	90.23 ± 1.54	0.87
			β_1	81.11 ± 1.63	1
			β_2	94.22 ± 1.35	0.59
	C_{101} S_γ	Fe_1	α_1	89.7 ± 1.40	0.81
			β_1	82.91 ± 1.54	1
			β_2	90.98 ± 1.84	0.46
	C_{110} S_γ	Fe_2	α_1	75.88 ± 1.81	1
			β_1	88.25 ± 1.22	0.98
			α_2	89.65 ± 1.71	0.32
	H_{114} N_δ	Fe_2	α_1	82.47 ± 1.23	1
			β_1	91.06 ± 1.24	0.21

Table S7
[2Fe-2S] cluster-binding domain bond properties upon HIS:Nε protonation in the mNT protein. See Table 6 for the description of the numerical parameters reported in these tables.

	Protein	Cofactor	Spin-BO	Δ	Occurrence
A	Protonated state				
	C_{72} S_γ	Fe_1	α_1	87.57 ± 1.19	0.98
			β_1	75.70 ± 1.61	1
			β_2	88.99 ± 1.52	0.87
	C_{74} S_γ	Fe_1	α_1	87.23 ± 1.03	0.99
			β_1	75.72 ± 1.19	1
			β_2	88.28 ± 1.77	0.97
	C_{83} S_γ	Fe_2	α_1	74.88 ± 1.43	1
			β_1	86.27 ± 0.77	1
			α_2	89.15 ± 1.77	0.95
	H_{87} N_δ	Fe_2	α_1	87.35 ± 1.18	0.99
B	Deprotonated state				
	C_{72} S_γ	Fe_1	α_1	89.10 ± 1.64	0.94
			β_1	76.03 ± 1.53	1.00
			β_2	90.48 ± 1.35	0.64
	C_{74} S_γ	Fe_1	α_1	87.94 ± 1.43	0.87
			β_1	76.13 ± 1.32	1.00
			β_2	88.32 ± 2.15	0.99
	C_{83} S_γ	Fe_2	α_1	74.42 ± 1.52	1.00
			β_1	87.81 ± 0.81	0.99
			α_1	91.23 ± 1.64	0.85
	H_{87} N_δ	Fe_2	α_1	84.77 ± 0.98	1.00
			β_1	91.72 ± 0.27	0.15

Table S8

Fe-N_δ Boys orbital polarization in mNT. The polarization is here measured as the distance between Boys orbitals centroids (BOCs) and N_δ. The BOCs distances from N_δ (Val) in the presence (yes) and in the absence (no) of coordinating histidine N_ε proton (His:N_ε-H), nearest water molecules to the coordinating sites (Wat), Lys55 (Lys) and protein environment (Env). The distances are reported for both α and β electron populations (Pop). The H-bond column (where specified) indicates the H-bonding partner (Lys55 or water) of the N_ε.

His:Nϵ-H	Wat	Lys	Env	Pop	H-bond	Val [Ang]
no	no	no	no	α		0.533 ± 0.016
				β		0.447 ± 0.014
yes	no	no	no	α		0.473 ± 0.011
				β		0.404 ± 0.008
no	yes	no	no	α		0.529 ± 0.016
				β		0.443 ± 0.011
yes	yes	no	no	α		0.481 ± 0.010
				β		0.409 ± 0.008
no	yes	yes	no	α		0.504 ± 0.014
					Lys	0.501 ± 0.012
					Wat	0.511 ± 0.014
				β		0.430 ± 0.012
					Lys	0.430 ± 0.010
					Wat	0.433 ± 0.012
no	yes	yes	yes	α		0.547 ± 0.019
				β		0.453 ± 0.013
yes	yes	no	yes	α		0.502 ± 0.010
				β		0.421 ± 0.009

Table S9

[2Fe-2S] cluster-binding domain bond properties upon His:Nε protonation in mNT and NAF-1 proteins without the protein environment. NBO analysis[22] (see methods) performed on the cluster-binding domain of NAF-1 for the His-protonated (A) and His-deprotonated (B) states and of mNT for the His-protonated (C) and His-deprotonated (D) states. Each row is related to a specific bond orbital estimated by the method. The first two columns are related to the protein and cofactor atoms involved in the specific bond. The third column is the spin and bond orbital order of the row. The fourth column provides mean values and standard deviations of the polarization (by the mean of NBO theory) of the specific molecular orbital, and the fifth column is the occurrence ratio (see SI text).

A

Protein	Cofactor	Spin-BO	Δ	Occurrence
Protonated state				
C_{99} S_γ	Fe_1	α_1	86.92 ± 0.81	1.00
		β_1	74.80 ± 1.45	1.00
		β_2	88.32 ± 1.72	1.00
C_{101} S_γ	Fe_1	α_1	86.99 ± 1.04	1.00
		β_1	75.41 ± 1.50	1.00
		β_2	87.33 ± 2.05	1.00
C_{110} S_γ	Fe_2	α_1	76.11 ± 1.32	1.00
		β_1	86.39 ± 0.73	1.00
		α_1	90.34 ± 1.80	0.94
H_{114} N_δ	Fe_2	α_1	88.67 ± 1.20	0.94

B

Protein	Cofactor	Spin-BO	Δ	Occurrence
Deprotonated state				
C_{99} S_γ	Fe_1	α_1	88.59 ± 1.21	1.00
		β_1	75.9 ± 1.74	1.00
		β_2	90.74 ± 1.49	0.87
C_{101} S_γ	Fe_1	α_1	87.91 ± 1.12	0.94
		β_1	77.70 ± 1.27	1.00
		β_2	89.40 ± 1.72	0.99
C_{110} S_γ	Fe_2	α_1	75.22 ± 1.31	1.00
		β_1	87.90 ± 0.80	1.00
		α_2	91.44 ± 1.46	0.91
H_{114} N_δ	Fe_2	α_1	85.87 ± 0.94	1.00
		β_1	91.97 ± 0.15	0.04

C

Protein	Cofactor	Spin-BO	Δ	Occurrence
Protonated state				
C_{72} S_γ	Fe_1	α_1	86.94 ± 0.85	1.00
		β_1	74.47 ± 1.60	1.00
		β_2	88.07 ± 1.75	0.99
C_{74} S_γ	Fe_1	α_1	87.07 ± 0.79	1.00
		β_1	75.78 ± 1.19	1.00
		β_2	87.34 ± 1.87	0.99
C_{83} S_γ	Fe_2	α_1	76.02 ± 1.29	1.00
		β_1	86.39 ± 0.69	1.00
		α_1	90.29 ± 1.59	0.95
H_{87} N_δ	Fe_2	α_1	88.82 ± 1.20	0.94

D

Protein	Cofactor	Spin-BO	Δ	Occurrence
Deprotonated state				
C_{72} S_γ	Fe_1	α_1	88.62 ± 1.28	1.00
		β_1	75.84 ± 1.55	1.00
		β_2	90.55 ± 1.57	0.85
C_{74} S_γ	Fe_1	α_1	87.85 ± 0.96	0.98
		β_1	77.79 ± 1.33	1.00
		β_2	89.62 ± 2.05	1.00
C_{83} S_γ	Fe_2	α_1	75.79 ± 1.27	1.00
		β_1	88.06 ± 0.75	1.00
		α_2	91.76 ± 1.39	0.83
H_{87} N_δ	Fe_2	α_1	85.92 ± 0.96	1.00
		β_1	91.98 ± 0.08	0.02

References

1. (a) Lindorff-Larsen, K.; Piana, S.; Palmo, K.; Maragakis, P.; Klepeis, J. L.; Dror, R. O.; Shaw, D. E., Improved side-chain torsion potentials for the Amber ff99SB protein force field. *Proteins* **2010,** *78* (8), 1950-8; (b) Sorin, E. J.; Pande, V. S., Exploring the helix-coil transition via all-atom equilibrium ensemble simulations. *Biophys J* **2005,** *88* (4), 2472-93.
2. Carvalho, A. T.; Teixeira, A. F.; Ramos, M. J., Parameters for molecular dynamics simulations of iron-sulfur proteins. *J Comput Chem* **2013,** *34* (18), 1540-8.
3. (a) Paddock, M. L.; Wiley, S. E.; Axelrod, H. L.; Cohen, A. E.; Roy, M.; Abresch, E. C.; Capraro, D.; Murphy, A. N.; Nechushtai, R.; Dixon, J. E.; Jennings, P. A., MitoNEET is a uniquely folded 2Fe 2S outer mitochondrial membrane protein stabilized by pioglitazone. *Proc Natl Acad Sci U S A* **2007,** *104* (36), 14342-7; (b) Tamir, S.; Eisenberg-Domovich, Y.; Conlan, A. R.; Stofleth, J. T.; Lipper, C. H.; Paddock, M. L.; Mittler, R.; Jennings, P. A.; Livnah, O.; Nechushtai, R., A point mutation in the [2Fe-2S] cluster binding region of the NAF-1 protein (H114C) dramatically hinders the cluster donor properties. *Acta Crystallogr D Biol Crystallogr* **2014,** *70* (Pt 6), 1572-8.
4. Peters, M. B.; Yang, Y.; Wang, B.; Fuesti-Molnar, L.; Weaver, M. N.; Merz, K. M., Jr., Structural Survey of Zinc-Containing Proteins and Development of the Zinc AMBER Force Field (ZAFF). *J. Chem. Theory Comput.* **2010,** *6* (9), 2935-2947.
5. Wiley, S. E.; Murphy, A. N.; Ross, S. A.; van der Geer, P.; Dixon, J. E., MitoNEET is an iron-containing outer mitochondrial membrane protein that regulates oxidative capacity. *Proc Natl Acad Sci U S A* **2007,** *104* (13), 5318-23.
6. Frisch, M. J.; Trucks, G. W.; Schlegel, H. B.; Scuseria, G. E.; Robb, M. A.; Cheeseman, J. R.; Scalmani, G.; Barone, V.; Mennucci, B.; Petersson, G. A.; Nakatsuji, H.; Caricato, M.; Li, X.; Hratchian, H. P.; Izmaylov, A. F.; Bloino, J.; Zheng, G.; Sonnenberg, J. L.; Hada, M.; Ehara, M.; Toyota, K.; Fukuda, R.; Hasegawa, J.; Ishida, M.; Nakajima, T.; Honda, Y.; Kitao, O.; Nakai, H.; Vreven, T.; Montgomery Jr, J. A.; Peralta, J. E.; Ogliaro, F.; Bearpark, M. J.; Heyd, J.; Brothers, E. N.; Kudin, K. N.; Staroverov, V. N.; Kobayashi, R.; Normand, J.; Raghavachari, K.; Rendell, A. P.; Burant, J. C.; Iyengar, S. S.; Tomasi, J.; Cossi, M.; Rega, N.; Millam, N. J.; Klene, M.; Knox, J. E.; Cross, J. B.; Bakken, V.; Adamo, C.; Jaramillo, J.; Gomperts, R.; Stratmann, R. E.; Yazyev, O.; Austin, A. J.; Cammi, R.; Pomelli, C.; Ochterski, J. W.; Martin, R. L.; Morokuma, K.; Zakrzewski, V. G.; Voth, G. A.; Salvador, P.; Dannenberg, J. J.; Dapprich, S.; Daniels, A. D.; Farkas, Ö.; Foresman, J. B.; Ortiz, J. V.; Cioslowski, J.; Fox, D. J. Gaussian 09 Revision E.01. 2009.
7. Becke, A. D., Density-functional thermochemistry. III. The role of exact exchange. *J. Chem. Phys.* **1993,** *98* (7), 5648-5652.
8. Giammona, D. A., Ph.D. Thesis. *Ph.D. Thesis, University of California: Davis* **1984**.
9. Ulrich, E.; Lalith, P.; L., B. M.; Tom, D.; Hsing, L.; G., P. L., A smooth particle mesh Ewald method. *J Chem Phys* **1995,** *102* (19), 8577-8593.
10. Hess, B.; Bekker, H.; Berendsen, H. J. C.; Fraaije, J., LINCS: A linear constraint solver for molecular simulations. *J. Comput. Chem.* **1997,** *18* (12), 1463-1472.
11. Hockney, R. W.; Goel, S. P.; Eastwood, J. W., Quiet high-resolution computer models of a plasma. *Journal of Computational Physics* **1974,** *14* (2), 148-158.
12. (a) Nose, S., A molecular dynamics method for simulations in the canonical ensemble. *Mol. Phys.* **1984,** *52* (2), 255-268; (b) Hoover, W. G., Canonical dynamics: Equilibrium phase-space distributions. *Phys. Rev. A* **1985,** *31* (3), 1695-1697.
13. Parrinello, M.; Rahman, A., Polymorphic transitions in single crystals: A new molecular dynamics method. *J. Appl. Phys.* **1981,** *52* (12), 7182-7190.

14. (a) Cerny, V., Thermodynamical approach to the traveling salesman problem: An efficient simulation algorithm. *J. Optim. Theory Appl.* **1985,** *45* (1), 41-51; (b) Kirkpatrick, S.; Gelatt, C. D.; Vecchi, M. P., Optimization by Simulated Annealing. *Science* **1983,** *220* (4598), 671-680.
15. Wang, L.; Friesner, R. A.; Berne, B. J., Replica exchange with solute scaling: a more efficient version of replica exchange with solute tempering (REST2). *J Phys Chem B* **2011,** *115* (30), 9431-8.
16. (a) Berendsen, H. J. C.; Vanderspoel, D.; Vandrunen, R., GROMACS - A message-passing parallel molecular dynamics implementation. *Comput. Phys. Commun.* **1995,** *91* (1-3), 43-56; (b) Hess, B.; Kutzner, C.; van der Spoel, D.; Lindahl, E., GROMACS 4: Algorithms for highly efficient, load-balanced, and scalable molecular simulation. *J. Chem. Theory Comput.* **2008,** *4* (3), 435-447.
17. Caliandro, R.; Rossetti, G.; Carloni, P., Local Fluctuations and Conformational Transitions in Proteins. *J Chem Theory Comput* **2012,** *8* (11), 4775-85.
18. D.A. Case, D. S. C., T.E. Cheatham, III, T.A. Darden, R.E. Duke, T.J. Giese, H. Gohlke, A.W. Goetz, D. Greene, N. Homeyer, S. Izadi, A. Kovalenko, T.S. Lee, S. LeGrand, P. Li, C. Lin, J. Liu, T. Luchko, R. Luo, D. Mermelstein, K.M. Merz, G. Monard, H. Nguyen, I. Omelyan, A. Onufriev, F. Pan, R. Qi, D.R. Roe, A. Roitberg, C. Sagui, C.L. Simmerling, W.M. Botello-Smith, J. Swails, R.C. Walker, J. Wang, R.M. Wolf, X. Wu, L. Xiao, D.M. York and P.A. Kollman, *AMBER 2017, University of California, San Francisco* **2017**.
19. Han, B.; Liu, Y. F.; Ginzinger, S. W.; Wishart, D. S., SHIFTX2: significantly improved protein chemical shift prediction. *Journal of Biomolecular Nmr* **2011,** *50* (1), 43-57.
20. Foster, J. M.; Boys, S. F., Canonical Configurational Interaction Procedure. *Reviews of Modern Physics* **1960,** *32* (2), 300-302.
21. (a) Arif, W.; Xu, S.; Isailovic, D.; Geldenhuys, W. J.; Carroll, R. T.; Funk, M. O., Complexes of the outer mitochondrial membrane protein mitoNEET with resveratrol-3-sulfate. *Biochemistry* **2011,** *50* (25), 5806-11; (b) Neese, F., The ORCA program system. *Wiley Interdiscip. Rev.-Comput. Mol. Sci.* **2012,** *2* (1), 73-78.
22. Reed, A. E.; Curtiss, L. A.; Weinhold, F., Intermolecular interactions from a natural bond orbital, donor-acceptor viewpoint. *Chem. Rev.* **1988,** *88* (6), 899-926.
23. Delaglio, F.; Grzesiek, S.; Vuister, G. W.; Zhu, G.; Pfeifer, J.; Bax, A., NMRPipe: a multidimensional spectral processing system based on UNIX pipes. *Journal of biomolecular NMR* **1995,** *6* (3), 277-93.
24. Goddard, T. D.; Kneller, D. G., SPARKY 3. University of California, San Francisco.
25. (a) Jennings, P. A., *Personal Communication* **2016**; (b) Zhou, T.; Lin, J.; Feng, Y.; Wang, J., Binding of reduced nicotinamide adenine dinucleotide phosphate destabilizes the iron-sulfur clusters of human mitoNEET. *Biochemistry* **2010,** *49* (44), 9604-12.
26. Calligari, P.; Gerolin, M.; Abergel, D.; Polimeno, A., Decomposition of Proteins into Dynamic Units from Atomic Cross-Correlation Functions. *J Chem Theory Comput* **2017,** *13* (1), 309-319.
27. Kabsch, W.; Sander, C., Dictionary of Protein Secondary Structure: Pattern Recognition of Hydrogen-Bonded and. Geometrical Features. *Biopolymers* **1983,** *22* (12), 2577-2637.
28. Reed, A. E.; Weinhold, F., Natural bond orbital analysis of near-Hartree–Fock water dimer. *J. Chem. Phys.* **1983,** *78* (6), 4066-4073.